Evaluation of a random displacement model for predicting particle escape from canopies using a simple eddy diffusivity model

Evaluation of a random displacement model for predicting particle escape from canopies using a simple eddy diffusivity model

Elizabeth Follett[a]*, Marcelo Chamecki[b], Heidi Nepf[a]

a. Department of Civil and Environmental Engineering, Massachusetts Institute of Technology, 77 Massachusetts Avenue Room 1-290, Cambridge, MA, 02139, USA

E-mail: emf@mit.edu, hmnepf@mit.edu

b. Department of Meteorology, The Pennsylvania State University, 503 Walker Building, University Park, PA, 16802, USA

E-mail: chamecki@psu.edu

*Corresponding author: Tel.: +1 (847) 471-8878, Fax: +1 (817) 258-8850

Abstract

There is a need for more practical tools for estimating spore escape from crop canopies, which is essential in forecasting the propagation of disease to other fields. In this paper, we evaluated whether a random displacement model (RDM) parameterized with an eddy diffusivity $K_z(z)$ could be used to predict spore escape probability. The proposed RDM does not require detailed turbulence measurements for parameterization. Instead, it constructs profiles of velocity and eddy diffusivity from a simple set of parameters [canopy height, canopy density, vegetation length scale, and wind speed]. The RDM was validated using field measurements of spore concentration. On average, the model predictions matched the field measurements within 28% inside the canopy and 42% above it, comparable to LES results over the same canopy. Once validated, the RDM was used to explore particle escape across a range of canopy densities and particle settling velocities, in order to inform estimates of particle escape from crops of varying maturity or area density. Escape fraction as calculated by the RDM increased as canopy density decreased, as the ratio of particle settling velocity to turbulent shear velocity ratio decreased, and as the source height within the canopy increased.

Keywords: particle transport; escape of particles from canopy; eddy diffusivity; random displacement model; maize

1. Introduction

Fungicides are used in agricultural production to reduce losses due to fungal disease. Unfortunately, some fungicide components are transported into freshwater systems, causing sub-lethal effects on ecosystem processes, including fish reproduction and leaf decomposition (Elskus, 2012). Therefore, for both economic and ecologic reasons, it is desirable to reduce the amount of fungicides applied to crops, while maintaining their benefits to crop yield. Integrated Pest Management (IPM) reduces fungicide use by targeting applications to when the pathogen is most vulnerable (Roberts and Reigart, 2013). Because chemical treatments are most effective during the first stages of fungal infection, it is necessary to forecast the spread of fungal spores to effectively time fungicide applications (Aylor, 1999). Therefore, an understanding of spore aerial transport is essential to the development of IPM strategies (Aylor and Irwin, 1999). For example, by correctly forecasting low soybean rust inoculum production and transport, the Integrated Aerobiology Monitoring System (IAMS) saved US soybean producers between $11 and $229 million in fungicide costs in 2005 (Isard et al., 2007). Evaluation of long distance spore transport must integrate the fungal life cycle, including spore release, escape from the canopy, transport and survival in the atmosphere, deposition on a new host, and infection of the host to generate new spores (Aylor 1986, 1990). This paper examines spore escape from the canopy, which depends on physical factors that determine the relative importance to spore escape of turbulent transport within the canopy, promoting escape, and spore settling, promoting deposition to the canopy and ground (e.g. Aylor and Taylor, 1983, Aylor, 1999, Aylor and Flesch, 2001, Nathan and Katul, 2005).

The vertical structure of turbulence within a canopy is dependent on the canopy morphology, which is characterized by the canopy height (h) and the plant frontal area per unit canopy volume (a_f). The dimensionless canopy density, or roughness density, is defined as $a_f h$. If the canopy density is high ($a_f h \gtrsim 0.1$), like most terrestrial crops, the drag imparted by the canopy is sufficient to generate an inflection point in the velocity profile, which leads to the generation of canopy-scale coherent structures at the top of the canopy through the Kelvin-Helmholtz instability (Raupach et al., 1996, Nepf, 2012). The canopy-scale vortices dominate the vertical turbulent transport of momentum and scalars, including spores, at the top of the canopy (Shaw et al., 1983; Ghisalberti and Nepf, 2005, 2006, Thomas and Foken, 2007). The region of the canopy flushed by these vortices is termed the exchange zone. The exchange zone extends from the top of the canopy over a distance $\delta_e = (0.23 \pm 0.06)/(C_D a_f)$, called the penetration length scale, with C_D the canopy drag coefficient defined using a quadratic drag that includes the prefactor ½ (Nepf et al., 2007).

Below the exchange zone exists a relatively quiescent region, termed the wake zone, within which turbulence is dominated by stem scale wakes, so that the vertical transport is greatly diminished relative to that in the exchange zone (Nepf et al., 2007). Because of the difference in vertical turbulent transport, spores originating in the wake zone, i.e., below the penetration of canopy-scale vortices, should have less likelihood of escaping the canopy than spores originating in the exchange zone, which can be flushed out by the canopy-scale vortices. Since the exchange zone decreases with increasing canopy density, the escape fraction should also decrease with increasing

canopy density. The likelihood of particle escape also depends on the particle's size and density, which dictate its settling velocity, w_s (Aylor, 1990, Aylor, 1999).

Some researchers (e.g. Pan et al., 2014) have simulated particle transport in canopy flow using large eddy simulation (LES), which resolves large scales of turbulence, but represents the impact of small-scale turbulence using sub-grid scale parameterization. However, LES requires significant time and computational resources, precluding the investigation of a wide parameter space. For a less computationally intensive approach, researchers have proposed various forms of Lagrangian stochastic models (LSM), which produce ensembles of stochastic spore trajectories. Turbulence is represented through second or third-order turbulent correlations, which are typically parameterized using measured profiles of velocity variance, turbulent momentum flux, and TKE dissipation rate (Aylor, 1990, de Jong et al., 1991, Aylor and Flesch, 2001, de Jong, 1992, Andrade et al., 2009). In this paper we propose a random displacement model (RDM) that uses an eddy diffusivity to represent turbulent transport. The proposed RDM does not require the measurement of detailed velocity statistics or significant computational resources, so that it could be a valuable tool for driving models of long-range spore transport by providing rapid estimation of escape fraction from crops of varying maturity or area density. This approach assumes that turbulent motions are uncorrelated, so that the time averaged turbulent fluxes act as an enhanced Fickian diffusion, described by a turbulent diffusion coefficient K_z (Legg and Powell, 1979, Aylor, 1982, Aylor, 1990, Aylor and Taylor, 1983, Denmead and Bradley, 1987). Because spores are released over hours, which is long compared to the duration of individual sweeps and ejections (6 to 10 s, Denmead and Bradley, 1987, Chamecki, 2013), an

uncorrelated model should reasonably represent the time-averaged escape behavior. Previous work has estimated eddy diffusivity from a canopy heat balance, or by using second-order turbulence statistics to represent the time-mean eddy diffusivity, $K_z = \sigma_w^2 T_L$, with Lagrangian time scale $T_L = \frac{2\sigma_w^2}{C_0 \varepsilon}$, with c_0 a universal constant and ε the rate of turbulence dissipation (Durbin, 1983, Legg and Powell, 1979, Wilson and Sawford, 1996). However, these approaches require detailed, canopy-specific measurements of turbulence statistics. In the proposed RDM, the velocity and eddy diffusivity profiles within and above a canopy were constructed from existing equations for a neutral boundary layer using a simple set of parameters [canopy height, canopy density, vegetation length scale, and wind speed]. The RDM performance was evaluated through a comparison to measured field data. After validation, the RDM was used to explore the trends in escape fraction over a range of canopy densities ($C_D a_f h = 0.1$ to 7), a range of settling velocities w_s/u_* (0 to 1), and as a function of particle source height, z_{src}/h (0 to 1, subscript 'src' denotes 'source').

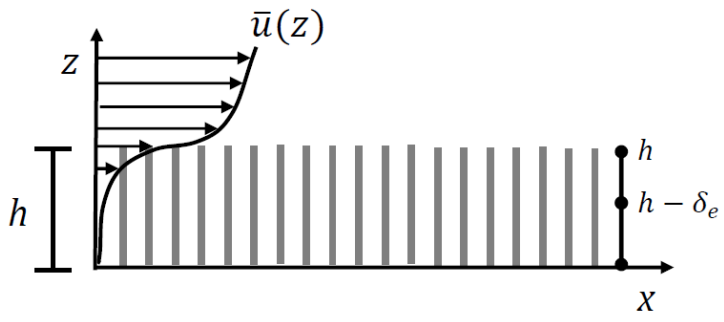

Figure 1 Schematic diagram of the lower part of the model domain, which extends to $z = 10h$. The longitudinal direction is x, the vertical direction is z, with $z = 0$ at the ground, the canopy height is h, and the time-averaged longitudinal velocity is $\bar{u}(z)$.

2. Methods

The RDM simulated a 2D domain (Figure 1) with the coordinates x and z parallel and normal to the ground, respectively. The velocity vector $\vec{u} = (u, w)$ corresponded to the streamwise and vertical coordinates (x, z), respectively. The time average and turbulent components of velocity were denoted by an overbar (e.g. $\bar{u}$) and prime (e.g. u'), respectively. Individual particles originated at a specific source height, z_{src}, within the canopy (0 < z_{src}< *h*) and were tracked until they deposited on the canopy, settled to the ground, or left the modeling domain. Particles that reached $z/h = 10$ were assumed to have left the domain and were no longer tracked. The number of particles per run (1000) was selected based on the fact that results with 1000 particles differed from results with 10,000 particles by less than 5 percent. The size of the model domain (x, z) was 18*h* x 10*h*. The sensitivity of results to domain size was evaluated by comparing 10 runs with a domain of 18*h* x 10*h* to 10 runs with a domain of 200*h* x 10*h*. The difference between escape fraction values determined in the two domains was less than 2%, indicating that the domain size did not significantly affect model results.

In each constant time-step (Δt) the position of the particle (x_p, z_p) advanced longitudinally with the mean velocity $\bar{u}$ and vertically due to both settling (w_s) and turbulent transport (w'). The equations used to model the particle position were (Wilson and Sawford, 1996):

$$x_{p,i+1} = x_{p,i} + \bar{u}(z_{p,i})\Delta t \quad (1)$$

$$z_{p,i+1} = z_{p,i} + \left(\frac{dK_z(z_{p,i})}{dz} - w_s\right)\Delta t + R\sqrt{2K_z(z_{p,i})\Delta t} \quad (2)$$

The last term in (2) represents transport by turbulent velocity $w' = R\sqrt{2K_z}/\sqrt{\Delta t}$, and *R* a random number drawn from a normal distribution with mean 0 and standard deviation 1. The vertical transport also included a drift correction, or pseudovelocity, associated with the vertical variation in diffusivity (dK_z/dz). The pseudovelocity term prevented the artificial accumulation of particles in regions of low diffusivity (Durbin, 1983, Boughton et al., 1987, Wilson and Sawford, 1996, Wilson and Yee, 2007). The formulations for the vertical profiles of time-mean streamwise velocity, $\bar{u}(z)$, and eddy diffusivity, $K_z(z)$ are described below in Section 2.1. The particle position was saved at every time-step. The model time-step, Δt, was constrained so that the vertical particle excursion within each time-step was much smaller than the scale of vertical gradients in the diffusivity and velocity (Israelsson et al., 2006). Within the model canopy, both the velocity and diffusivity varied over length scales of approximately 0.1*h*. For each run the time-step satisfied the following condition:

$$\Delta t < \min\left(\frac{0.1h}{\left|\frac{\partial K_z}{\partial z} - w_s\right|_{max}}, \frac{(0.1h)^2}{K_z|_{max}}\right). \quad (3)$$

Within each time-step, after a particle was moved, the position was assessed to determine if the particle had settled to the ground ($z_{p,i} = 0$); escaped the canopy ($z_{p,i} > h$); escaped the model domain ($z_{p,i} > 10h$ or $x_{p,i} > 18h$); or deposited to the canopy. For a continuous release, as considered here, the fraction of spores escaping the canopy is a function of distance from the source, but not time. As described in Pan et al. (2014), the escape fraction initially increases with distance from the source, reaching a maximum at $x/h = 2$ to 6, depending on settling velocity (Figure 7 in Pan et

al., 2014). Since the canopy is a sink for particles, over longer distances particles may return to the canopy through turbulent transport or settling and be deposited, so that at larger distances the escape fraction exhibits a slow decline with distance. To provide a single, consistent metric with which to compare different scenarios in Section 3.2, we adopt the escape fraction metric (EF) defined by Pan et al. (2014) as the maximum fraction of the released particles observed above the canopy.

Canopy deposition was described using a modified version of the model given in Aylor and Flesch (2001). Deposition on vertical facing and upward facing surfaces was possible if the velocity was less than the critical velocity $u_{crit} = 0.45$ m/s, determined by Aylor (2005) for pollen capture in a maize canopy. Particle rebound and re-entrainment was expected if the particle velocity was greater than u_{crit}. We caution that the value of u_{crit} may vary with particle type (pollen versus spores), and also with canopy rigidity and morphology. Following Pan et al. (2014), deposition on downward facing surfaces was neglected. Deposition on upward facing surfaces was possible if the particle had a negative vertical particle excursion, $z_{p,i+1} - z_{p,i} < 0$. The rate of deposition on an upward facing surface (S_u) was calculated as the product of the two-sided leaf area density, $a(z)$, the fractional projected leaf area normal to the vertical direction (P_z), and the settling velocity:

$$S_u = P_z a(z) w_s \tag{4}$$

Pan et al. (2014, eq. A2) described particle deposition to vertical surfaces in a three-dimensional domain. Here, we modified the formulation for the two-dimensional domain (x-z) of this RDM. Specifically, the projected area in the x direction was assumed to be

194 the sum of the measured projected leaf area facing the x (P_x) and y (P_y) directions in 3D
195 space ($P_{x,2D} = P_x + P_y$), and the rate of impaction depended only on the mean
196 longitudinal velocity ($\bar{u}$) since $\bar{v} = 0$ in the 2D domain. The rate of deposition on
197 vertical surfaces (S_v) is then given by:

198 $$S_v = EI\left(P_{x,2D}\right)a(z)\bar{u} \quad (5)$$

199 with impaction efficiency (*EI*),

200 $$EI = 0.86(1 + 0.442St^{-1.967})^{-1} \quad (6)$$

201 based on Aylor (1982). In eq. (6), St is the Stokes number $St = \frac{w_s\bar{u}}{gL_v}$, with L_v the
202 characteristic length scale of the canopy elements and *g* the gravitational acceleration.
203 Because the RDM tracked individual particles, the time rate of deposition given by (4)
204 through (6) was converted to a probability for individual particle deposition during one
205 time-step. Following Aylor (1989), the rate of deposition, $S_u + S_v$, was multiplied by Δt,
206 resulting in a number between 0 and 1 that represented the probability of deposition
207 during that time-step. The need to keep the fraction of particles deposited in each time-
208 step less than 1 imposed an additional constraint on the time-step; however, this
209 condition was satisfied by the more stringent constraints on the vertical particle
210 excursion (eq. 3). To determine if the particle deposited during the time-step, a random
211 number, R_c, was chosen from a uniform distribution between 0 and 1. If R_c was less
212 than or equal to the probability of deposition, the particle deposited to the canopy.

213

214 **2.1. Velocity and Eddy Diffusivity Profiles to Parameterize RDM**

Several previous studies were combined to describe $\bar{u}(z)$ and $K_z(z)$ as functions of only u_*, $a_f h$, h, L_v, and C_D. The friction velocity (u_*) is defined at the top of the canopy, ${u_*}^4 = \left(\overline{u'w'}\right)_h^2 + \left(\overline{v'w'}\right)_h^2$ (In this paper, the velocity field is assumed to be aligned with x and uniform in y, so that $\overline{v'w'} = 0$). Profiles were only constructed for dense canopies ($a_f h \gtrsim 0.1$), representative of most terrestrial crops. Within the canopy the profiles are divided into two regions. In the wake zone ($z < h - \delta_e$), both K_z and $\bar{u}$ are small, so particle transport is likely dominated by settling (w_s). In the exchange zone ($z \geq h - \delta_e$), canopy-scale vortices elevate K_z and contribute to greater momentum penetration from above, and thus higher $\bar{u}$, so that both turbulent transport and capture to the canopy may become important processes for spore transport.

First, the profile for the mean longitudinal velocity is described. Above a dense canopy, there is a displaced boundary-layer profile:

$$\bar{u}(z) = \frac{u_*}{\kappa} ln\left(\frac{z - z_m}{z_0}\right) \tag{7}$$

in which $\kappa = 0.4$ is the von Kármán constant (Raupach, 1994, Thom, 1971). The displacement height (z_m) and roughness height (z_0) are both functions of canopy density (e.g., Schlichting 1936, Grimmond and Oke, 1999). Following Luhar et al. (2008), the displacement height z_m and roughness height z_o can be described in terms of $C_D a_f h$,

$$\frac{z_m}{h} = 1 - \frac{0.12}{C_D a_f h} \tag{8}$$

$$\frac{z_o}{h} = 0.04\left(C_D a_f h\right)^{-1} \qquad C_D a_f h \geq 0.1 \tag{9}$$

The velocity inside the canopy follows an exponential decay, e.g. combining Harman and Finnigan (2007) and Nepf (2012):

$$\bar{u}(z) = u_1 + (u_h - u_1)e^{\frac{\beta(z-h)}{l}} \quad (10)$$

in which u_h is the velocity at the top of the canopy, and u_1 is the velocity in the lower canopy (wake zone), below the penetration of vertical turbulent momentum flux. The ratio u_1/u_h decreases with increasing canopy density, and the following relation was determined by fitting data from terrestrial canopies reported in Figure 1 and Table 1 in Finnigan (2000):

$$u_1/u_h = 0.16\left(a_f h\right)^{-0.68} \quad (11)$$

Given u_*, equations (7) to (9) predict the velocity at the top of the canopy, $u_h = u(h)$. Specifically, u_h/u_* = 2.7 for all values of a_f, which is consistent with observations made across a wide range of dense aquatic and terrestrial canopies (Ghisalberti, 2009). The velocity-decay length-scale (l/β in 10) can be determined using a mixing length (l) characterization of eddy viscosity, which leads to $\beta = \frac{u_*}{u_h}$ and $l = \frac{2\beta^3}{C_D a_f}$ (Harman and Finnigan, 2007).

Next, consider the vertical profile of eddy diffusivity. Previous parameterizations of eddy diffusivity, such as Massman and Weil (1999), do not reflect the contributions of the coherent structures at the top of the canopy, or the role of the plant-scale vortices within the canopy, both of which have been recently shown to provide important controls on the magnitude of diffusivity within the canopy (Poggi et al., 2004, Tanino and Nepf, 2008). The models used here incorporate both of these important length-scales. In the

wake zone ($z < h - \delta_e$), the diffusivity is dominated by plant-scale turbulence, and K_z scales on the characteristic vegetation length scale (L_v) and the velocity scale $\sqrt{k_t}$ associated with the turbulent kinetic energy (k_t) generated in the plant wakes (Raupach et al., 1996, Finnigan, 2000, Tanino and Nepf, 2008). Tanino and Nepf (2008) developed models for k_t and K_z as functions of canopy morphology (L_v and a_f) and local velocity ($\bar{u}$). Most crops have a low solid volume fraction ($\phi = a_f t$, with t the blade thickness), such that plant-scale eddies can exist throughout the canopy and have scale L_v, so that equations (2.12) and (2.15) in Tanino and Nepf (2008) reduce to:

$$\frac{K_z}{\bar{u} L_v} = 4.5 \left(\frac{\sqrt{k_t}}{\bar{u}} \right) \tag{12}$$

$$\frac{\sqrt{k_t}}{\bar{u}} = 1.1 \left(C_D \frac{a_f L_v}{2} \right)^{1/3} \tag{13}$$

in which the scale coefficients (1.1 and 4.5) were determined in laboratory experiments (Tanino and Nepf, 2008).

In the upper canopy ($h - \delta_e < z < h$), the flow resembles a mixing layer (Raupach et al., 1996), within which the eddy diffusivity follows a mixing length model (e.g. Poggi et al., 2004),

$$K_z(z) = \left(\frac{1}{Sc}\right) {l_{eff}}^2 \partial \bar{u} / \partial z \tag{14}$$

with effective eddy length-scale l_{eff}. The turbulent Schmidt number, Sc, was assumed to be equal to 0.5, as in a mixing layer (Raupach et al.,1996). This is consistent with recent laboratory experiments for which Sc equal to 0.47 was measured within and above a model canopy in a neutrally stable flow (Ghisalberti and Nepf, 2005). A range

of Sc values between 0.5 and 1 has been observed above crop canopies, with Sc increasing with atmospheric stability and dependent on scalar species (Wilson, 2013).

Using $u_h/u_* = 2.7$ (determined above), the velocity-decay length-scale in (10) is $l/\beta = 2\beta^2/C_D a_f = 0.27/(C_D a_f) \approx \delta_e$, such that it is reasonable to approximate $\partial u/\partial z\,|_{z=h} = u_h/\delta_e$ in (14). Thus, the diffusivity at the top of the canopy ($z = h$) is $K_h = 2{l_{eff}}^2 u_h/\delta_e$, which is the local maximum in diffusivity. For simplicity, a linear transition was assumed between K_h at $z = h$ and the lower canopy value given by eq. (12) at $z = h - \delta_e$. The contribution of the mixing-layer vortices to K_z was assumed to be symmetric about $z = h$, such that the eddy diffusivity decays over the same length scale, δ_e, above the canopy.

Following Poggi et al. (2004), the effective eddy length-scale (l_{eff}) is a combination of the mixing-layer (l_{ML}) and boundary-layer (l_{BL}) length scales:

$$l_{eff} = (1-\alpha) l_{BL} + \alpha l_{ML} \tag{15}$$

$$l_{BL} = \kappa(z - z_m) \tag{16}$$

$$l_{ML} = \frac{2}{C_D a_f}\beta^2 \tag{17}$$

The relative contribution of the mixing layer length scale (α) is a function of $C_D a_f h$. Figures 8 and 9 from Poggi et al. (2004) showed that α reached an asymptote of $\alpha = 0.45$ for $C_D a_f h \geq 0.6$, and $\alpha = 0.25$ to 0.45 over the range $C_D a_f h = 0.1 - 0.6$. Using $u_h/u_* = 2.7$ (determined above), $\beta = u_*/u_h = 0.37$, which leads to $l_{ML} = 0.27\left(C_D a_f\right)^{-1} \approx \delta_e$; i.e., the eddy length scale in the mixing layer corresponds to

the length scale of turbulence penetration into the canopy. Note that as $C_D a_f$ approaches zero, (17) implies that l_{ML} is unbounded, which is not physically reasonable. To correct this, l_{ML} is constrained to be the minimum of eq. (17) and *h*. Finally, above $z = h + \delta_e$, the eddy diffusivity follows the boundary-layer form,

$$K_z(z) = (\frac{1}{Sc})\kappa u_*(z - z_m) \qquad z > h + \delta_e \ , \tag{18}$$

with $Sc = 0.8$ for a boundary layer (Launder, 1976, Hassid, 1983, Koeltzch, 2000).

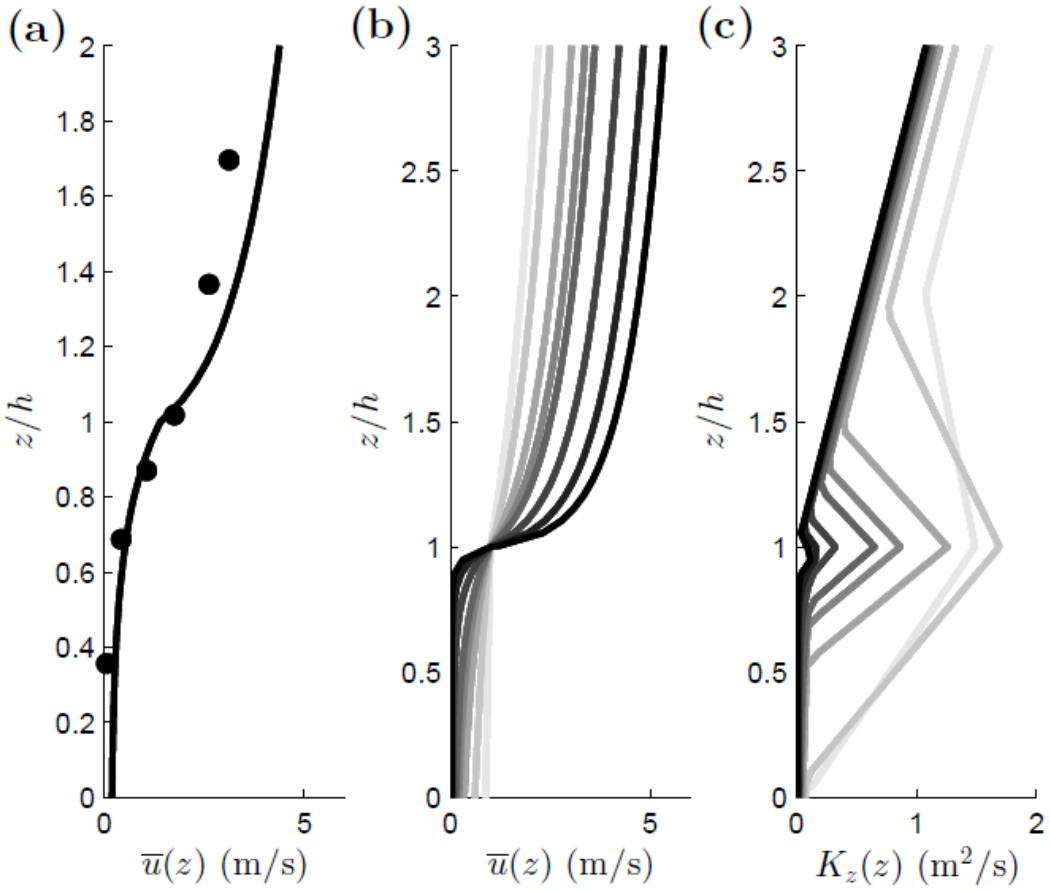

Figure 2 (a) time-averaged velocity $\overline{u}(z)$ (m/s) predicted from eqs. (7) to (10) shown by solid line and measured over a maize field (Gleicher et al., 2014), shown by dots. Family of curves describing (b) time-averaged streamwise velocity $\overline{u}(z)$ (m/s) and (c) vertical turbulent diffusivity $K_z(z)$ (m^2/s) predicted from eqs. (7) to (18). From light to dark, curves represent increasing canopy density, with $C_D a_f h = 0.1, 0.25, 0.5, 0.75, 1, 2, 4, \text{and } 7$, respectively, with $u_* = 0.51$ m/s,

$h = 2.1$ m, L_v =0.1m, and $C_D = 0.68$ for all curves, based on a maize canopy, as described in the text.

Figure 2a shows velocity measured in a maize field (dots) and the time-averaged velocity constructed from eqs. (7) through (10) using parameters from that maize field, specifically $u_* = 0.51$ m s^{-1}, $h = 2.1$ m, and $LAI = 3.3$. (Gleicher et al., 2014). Following Finnigan (2000), the frontal area density was assumed to equal ½ the one-sided leaf area index, $a_f h = \frac{1}{2} LAI$. Wilson et al. (1982) measured $C_D = 0.17$ for maize, but used a drag formulation that excludes the factor of $\frac{1}{2}$, which we include, and used the single-sided leaf area, whereas we use $\frac{1}{2} LAI$. To compensate, we adjusted C_D by a factor of 4, such that $C_D = 0.68$. Using only the reported values of u_*, h, C_D, and LAI the constructed velocity profile (solid line in Figure 2a) agreed with the measured velocity (dots in Figure 2a) to within 0.26 m/s inside the canopy ($z/h \leq 1$), and to within 0.85 m/s above the canopy ($1 < z/h \leq 1.7$).

Figures 2b and 2c show the family of curves constructed from eqs. (7) through (18) using $C_D a_f h = 0.1$ to 7. The velocity profiles resemble the family of measured velocity profiles shown in Figure 1 of Finnigan (2000). Recall that only dense canopies have been considered ($C_D a_f h > 0.1$), and consistent with this each velocity profile resembles a mixing layer, with a velocity inflection point at the top of the canopy. Importantly, the model captures the peak in diffusivity at the top of the canopy (Figure 2c) associated with the coherent structures formed in the mixing-layer, a feature that is not captured by the model proposed by Massman and Weil (1999). At the lowest densities considered (lightest lines), the coherent structures penetrate to the ground ($\delta_e = h$), elevating diffusivity over the full canopy. As canopy density increases, the

exchange zone decreases in size ($\delta_e \sim (C_D a_f)^{-1}$).The mixing layer eddy length-scale, $l_{ML} \sim (C_D a_f)^{-1}$, also decreases, leading to a diminished diffusivity at the top of the canopy.

Figure	w_s/u_*	$a_f h$	h (m)
2a	—	1.65	2.1
2b,c	—	$0.15 - 10.29$	2.1
3	0.04	1.65	2.1
4	$0.01 - 1$	1.65	2.1
5a-d	$0 - 5$	$0.15 - 10.29$	2.1
5e,f	$0, 0.1$	$0.15 - 10.29$	$0.067 - 4.67$
Gleicher et al. (2014)	0.04	1.65	2.1

$C_D = 0.68, u_* = 0.51$ m/s, $L_v = 0.1$ m in all figures

Table 1 Description of parameters used for each set of simulations

3. Results and Discussion

3.1 Validation using field data from maize canopy

The RDM was validated against measurements from a field release of *Lycopodium* spores ($w_s = 1.94$ cms^{-1}) in a maize canopy (Gleicher et al., 2014), which is the same study used for comparison in Figure 2a. Gleicher et al. (2014) report $u_* = 0.51$ m s^{-1}, $h = 2.1$ m, $LAI = 3.3$. The characteristic vegetation length scale is the leaf width, $L_v = 0.1$ m (Silva et al., 2012). Gleicher released spores from a single pole at three source heights ($\frac{z_{src}}{h} = 1, \frac{2}{3}, \frac{1}{3}$) and captured spores using a grid of 9 poles, with 5 rotorods per pole ($\frac{x}{h} = 0.94, 1.9, 3.8$, $\frac{y}{h} = -0.36, 0, 0.36$, $\frac{z}{h} = 0.34, 0.68, 1.0, 1.4, 1.7, h = 2.1$ m). Rotorod data was missing from three locations ($\frac{x}{h} = 1.9, 3.8, \frac{y}{h} = 0.36$), so data for

these three rotorod locations was taken from the corresponding rotorods at the opposite poles ($\frac{x}{h} = 1.9, 3.8, \frac{y}{h} = -0.36$).

We calculated concentration and airborne flux in the RDM using a method similar to Gleicher et al. (2014). A vertical column of interrogation boxes (0.2 m long x 0.1 m high) was defined, centered at the field data collection points. The particle concentration was found by dividing the number of airborne particles in each box by the box area. Particles were continuously released until a steady-state particle concentration was established in each box. Because RDM is two dimensional in *x*-*z,* it cannot represent the lateral dispersion present in the field. Therefore, the field data was adjusted to correct for the fraction of particles lost from the control volume by lateral dispersion. Specifically, the field data was normalized by the equivalent two-dimensional flux represented within the measurement volume, $Q_x = \int_{-0.76\ m}^{0.76\ m} \int_{0.7\ m}^{3.5\ m} \bar{u} C dz dy$), with the integral approximated by trapezoidal summation. A laterally-integrated concentration was found from the measurements at the three y locations ($\langle C \rangle = \int_{-0.76\ m}^{0.76\ m} C(x, y, z) dy$), which has units of spores m^{-2}. The concentration within the 2-D RDM was, by definition, the laterally-integrated value, $\langle C \rangle$. The RDM concentration was scaled by the two-dimensional flux at each x location ($Q_x = \int_{0.7\ m}^{3.5\ m} \bar{u} \langle C \rangle\ dz$, which has units of spores s^{-1}), with the integral approximated by trapezoidal sums. Using this method, both the RDM and field normalized flux profiles $\frac{\bar{u}\langle C \rangle}{Q_x}$ integrate to 1.

The field measurement (C_f) and predicted (C_p) spore concentrations are shown in Figure 3. With $\bar{u}(z)$ and $K_z(z)$ predicted from eqs. (7) to (18) using the measured

368 canopy parameters from Gleicher (summarized in Table 1), 73% of the predicted spore
369 concentrations were within a factor of 2 of the field observations ($FAC2 = 73\%$; fraction
370 of data that satisfy $0.5 \leq \frac{C_p}{C_f} \leq 2.0$) (Chang and Hanna, 2008). The agreement improved
371 with distance from the source (Figure 3g,h,i; Table 2), which is consistent with the
372 expectation that the RDM makes better predictions in the far-field. At the farthest
373 measurement point ($x/h = 3.8$), and for all source heights, the prediction
374 concentrations were, on average, 1.28 times the field measurements within the canopy
375 and 0.58 times the field measurements above it. The underprediction of concentration
376 above the canopy may have been related to the overprediction of $\bar{u}$ in this region (see
377 Figure 2a).

378 For additional comparisons, the geometric mean bias (VG) and ratio of geometric
379 means, or mean geometric bias (MG) were also assessed (Hanna et al., 1993, Chang
380 and Hanna, 2004):

381 $$VG = e^{\left(ln\frac{\widetilde{C_f}}{\widetilde{C_p}}\right)^2} \quad (19)$$

382 $$MG = e^{\widetilde{lnC_f} - \widetilde{lnC_p}} \quad (20)$$

383 in which the tilde indicates the spatial average over all rotorod heights. Chang and
384 Hanna (2004) suggest that a "good" model should have greater than 50% of model
385 predictions within a factor of 2 of observations ($FAC2 > 50\%$), a geometric mean bias
386 (VG) less than 1.6, and a ratio of geometric means within 30% ($0.7 < MG < 1.3$). The
387 $FAC2$, VG, and MG values for each measurement location and release height are shown
388 in Table 2. All statistics improved with x/h, approaching or exceeding the

389 recommendation from Chang and Hanna (2004). The geometric mean bias, which
390 reflected the ratio between C_f and C_p on a logarithmic scale, was unacceptably large for
391 $x/h = 0.95, 1.9$, suggesting an initially lower dispersion of the RDM relative to the field
392 measurements. By $x/h = 3.8$, all statistics were within the range of a "good" model
393 (Chang and Hanna, 2004).

394 Recently, an LES model (Pan et al, 2014) and a first-order LSM with memory
395 terms (Gleicher et al., 2014) were compared to the same field release of *Lycopodium*
396 spores. The performance of all three models is compared in Table 2. At $x/h = 3.8$, the
397 RDM performed similarly to the LES and better than the LSM. Note that the LES
398 performance declined with source height (Table 2), and that the RDM performed better
399 for z_{src}/h = 2/3 and 1/3. This is because the RDM included the contribution of plant-
400 scale eddies in the lower canopy (see eq. 12 and 13). The LES model used a
401 distributed drag to represent the canopy, which did not produce leaf-scale eddies and
402 their contribution to mass flux in the lower canopy, such that the LES underestimated
403 the diffusivity in the lower canopy. Consistent with this, below the penetration of canopy
404 scale vortices ($z \leq h - \delta_e$), the far field eddy diffusivity (derived by dividing the LES local
405 mean vertical flux by the vertical gradient in mean concentration) was 6 times smaller
406 than the eddy diffusivity predicted by eqs. (12) and (13), which was used in the RDM.
407 Because the region below the penetration of canopy scale vortices comprises a
408 significant fraction of dense canopies, it is important to correctly represent vertical
409 transport in this region. The performance of the LES in the lower canopy might be
410 improved by incorporating eq. (13) to represent the contribution of unresolved, plant-
411 scale eddies.

Because the RDM does not resolve individual sweeps and ejections, it can only model far field particle behavior, after particles have been in transport for more than 10 Lagrangian timescales ($\tau_l \cong 0.28 - 0.63$ s, based on velocity measurements of the Eulerian integral time scale made during the same maize field study, Chamecki, 2013). To explore at what point far field conditions began in the RDM, the transport time for airborne particles to reach several x locations was tracked. The far-field condition was reached at $x/h = 5$, at which point over 95% of the airborne particles had been in transport for more than 10 Lagrangian timescales. Because the maximum escape in the RDM occurred beyond this point, an eddy diffusivity-based approach should adequately represent EF. This, together with the agreement between the modeled and measured spore concentrations, built confidence in the RDM model, which was next used to evaluate trends in EF with particle size (w_s/u_*) and canopy density ($C_D a_f h$).

z_{src}/h	statistic	$x/h = 0.95$	$x/h = 1.9$	$x/h = 3.8$	LES	LSM
1	$FAC2$	80%	80%	80%	93%	55%
	MG	1.52	1.43	1.17	1.02	1.87
	VG	1.79	1.27	1.20	1.17	2.05
2/3	$FAC2$	60%	80%	80%	70%	67%
	MG	2.07	1.56	1.09	0.70	1.13
	VG	19.5	2.18	1.37	1.42	1.80
1/3	$FAC2$	40%	80%	80%	66%	71%
	MG	2.78	1.51	1.09	1.09	1.02
	VG	153	2.50	1.39	2.18	1.45

Table 2 Fraction of RDM predictions within a factor of 2 of field observations (Gleicher et al., 2014) (*FAC2*), ratio of geometric means (*MG*), and geometric mean bias (*VG*) at three x/h locations and three source heights. Quantitative statistics representing the average value of the comparison to field data at all longitudinal locations ($x/h =$

0.95,1.9,3.8) are included for an LES model (Pan et al., 2014) and a first order Lagrangian stochastic model (Gleicher et al., 2014)

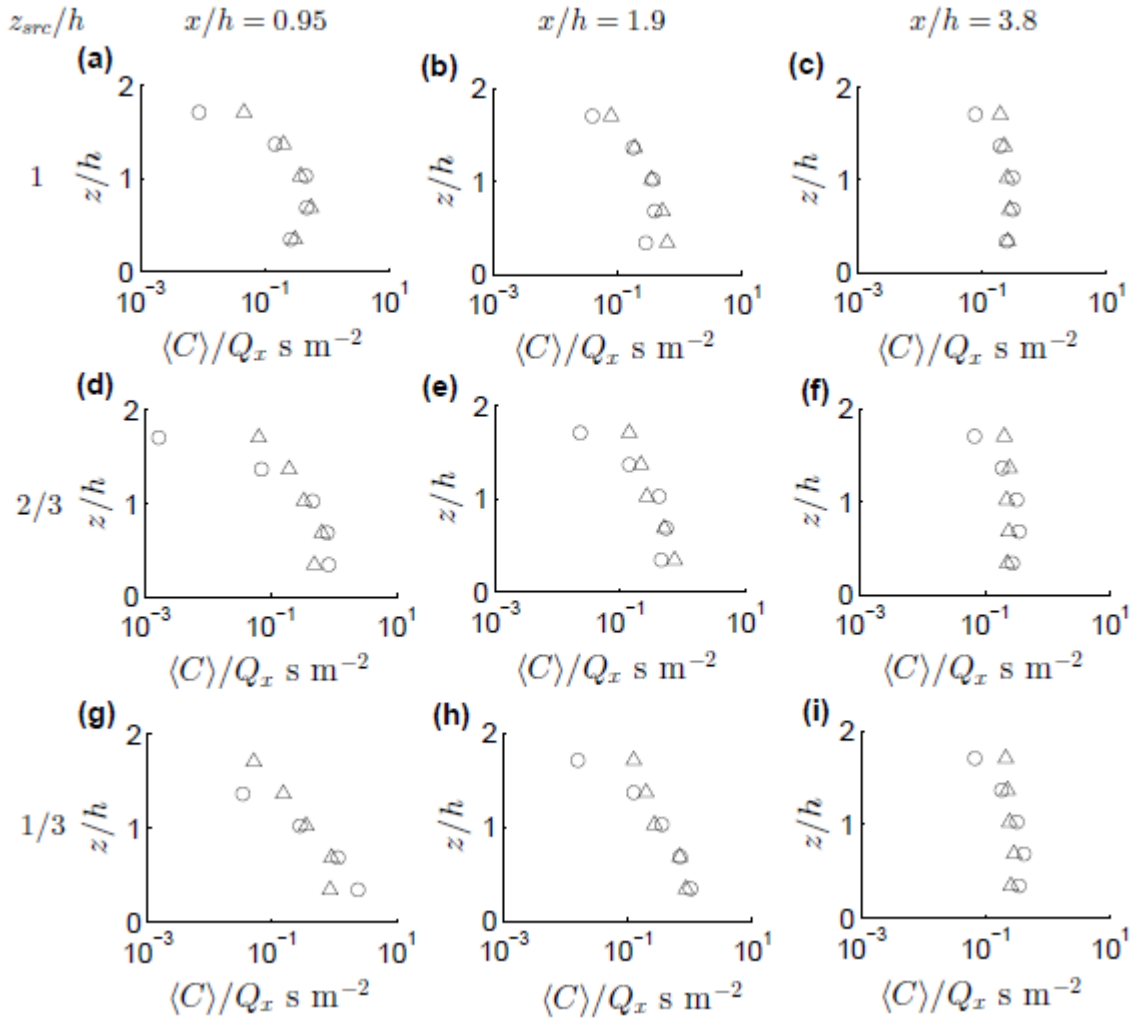

Figure 3 Comparison of the concentration predicted by RDM-maize (open circles) with measured concentration of *Lycopodium* spores released in a maize canopy (Gleicher et al., 2014), shown with open triangles. The laterally integrated concentration $\langle C \rangle$ is normalized by the equivalent source flux (Q_x), and vertical coordinate (z) is normalized by canopy height h. Spores were released at $z_{src}/h = 1/3$ (a, b, c), 2/3 (d, e, f), and 1 (g, h, i). The spores were collected at $x/h = 0.95$ (a,d,g), 1.9 (b,e,h), 3.8 (c,f,i).

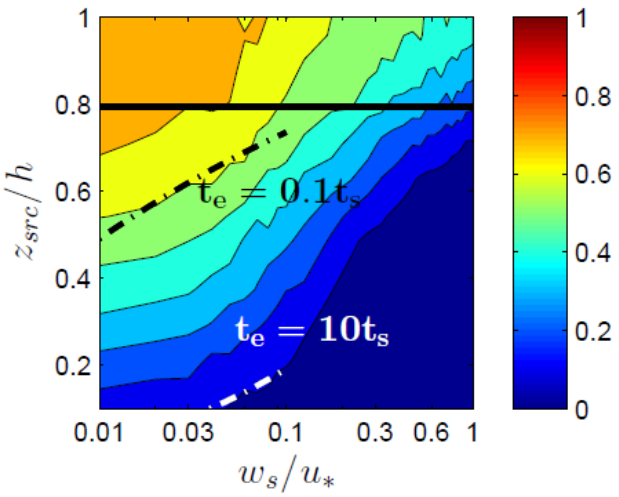

Figure 4 Particle escape fraction (EF, values shown in color bar) from a maize canopy ($LAI = 3.3$) as a function of the source height, z_{src}, normalized by canopy height *h*, and particle settling velocity w_s, normalized by friction velocity u_*. The solid black horizontal line denotes the depth of turbulence penetration from above ($z = h - \delta_e$). Lines comparing the time-scale of escape (t_e, eq. 20) and of settling (t_s, eq. 21) are also shown. The lines represent the locus in (z_{src}/h,w_s/u_*) space for which $t_e = \gamma t_s$ with $\gamma = 0.1$ (black dashed line) or 10 (white dashed line). The solid black contour lines separating regions of different color represent successively the EF contours 0.1 to 1 in intervals of 0.1.

3.2 Exploration of escape trends over w_s/u_*, $C_D a_f h$, h

RDM was used to explore how the velocity ratio (w_s/u_*), canopy density, and canopy height impacted escape fraction, an investigation of 1788 simulations (Figures 4,5) that would have been computationally prohibitive using LES methods. First, RDM was used to explore how the velocity ratio impacted escape fraction (Figure 4, model parameters given in Table 1). The solid horizontal line indicates the expected penetration of shear-layer turbulence from above the canopy, i.e. $z = h - \delta_e$. Consider particles with settling velocity comparable to the turbulent velocity ($w_s/u_* = 1$). These particles only escaped if they originated in the exchange zone ($z_{src} > h - \delta_e$), i.e. the region within which turbulent transport is enhanced by the canopy-scale vortices formed

458 at the top of the canopy. Escape from the wake zone ($z_{src} < h - \delta_e$) was unlikely
459 (<10%), because of the significantly lower K_z associated with the stem-scale vortices
460 that dominate transport in this region (eq. 12). In contrast, particles with relatively small
461 settling velocity ($w_s/u_* < 0.1$) could be moved significant distances by the lower canopy
462 turbulence, allowing escape even for particles originating deep within the canopy. For
463 these light particles ($w_s/u_* < 0.1$), canopy deposition was less important (impacting less
464 than 20% of the particles, data not shown), so that the trends in escape fraction could
465 be predicted by comparing the time scale for turbulent transport to the top of the canopy
466 (t_e) and the time scale for settling to the ground (t_s):

467 $$t_e = \frac{(h - z_{src})^2}{K_z(z_{src})} \quad (21)$$

468 $$t_s = \frac{z_{src}}{w_s} \quad (22)$$

469 Figure 4 depicts the locus in (z_{src}/h,w_s/u_*) space for which $t_e = \gamma t_s$ with $\gamma = 0.1$ (black
470 dashed line) and 10 (white dashed line). Escape was rare (<10%) if $t_e/t_s >> 1$,
471 corresponding to particles originating below the lower dashed line. Escape was
472 common (>60%) if $t_e/t_s << 1$, corresponding to the region above the upper dashed
473 line.

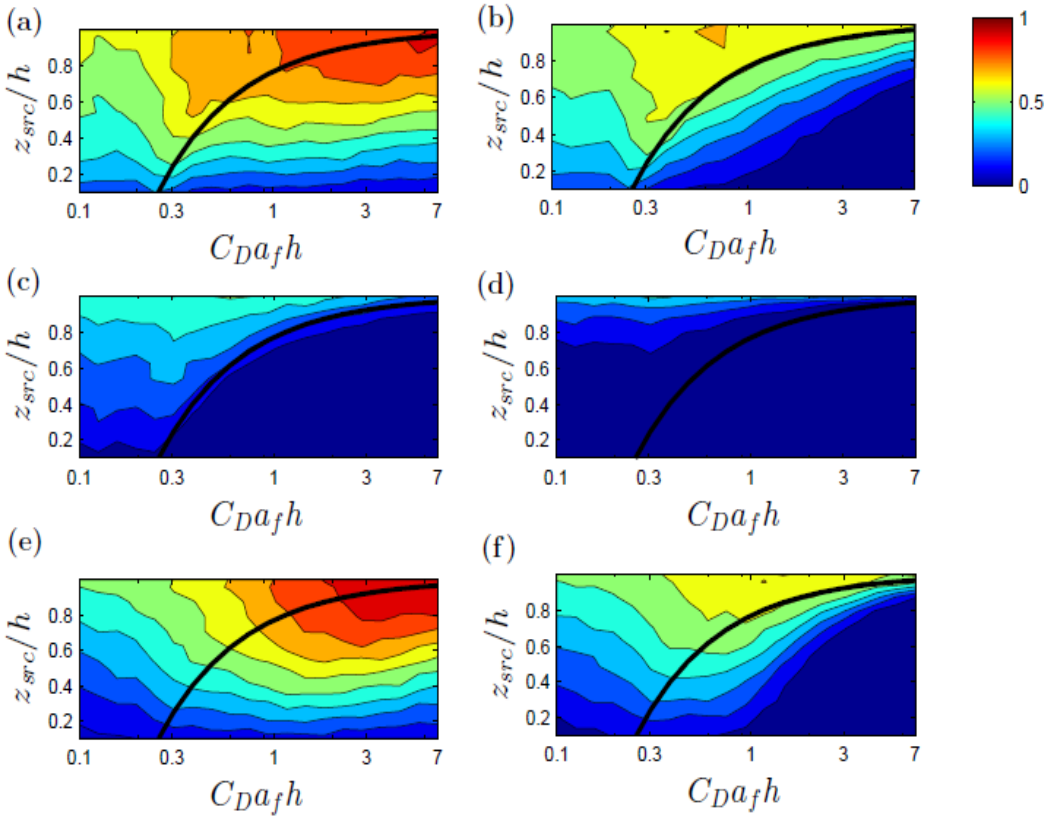

Figure 5 Escape fraction (*EF* = 0 to 1, as shown in color bar) as a function of source height z_{src} normalized by canopy height h and non-dimensional canopy density $C_D a_f h$. The penetration of turbulence from above extends to $z = h - \delta_e$, denoted by the thick black line in each subplot. For (a) to (d), $h = 2.1$ m with varying a_f, and $w_s/u_* = 0$ (a), $w_s/u_* = 0.1$ (b), $w_s/u_* = 1$ (c), $w_s/u_* = 5$ (d). For (e) and (f), $a_f = 0.79$ m^{-1} with varying *h*, and $w_s/u_* = 0$ (e), $w_s/u_* = 0.1$ (f).

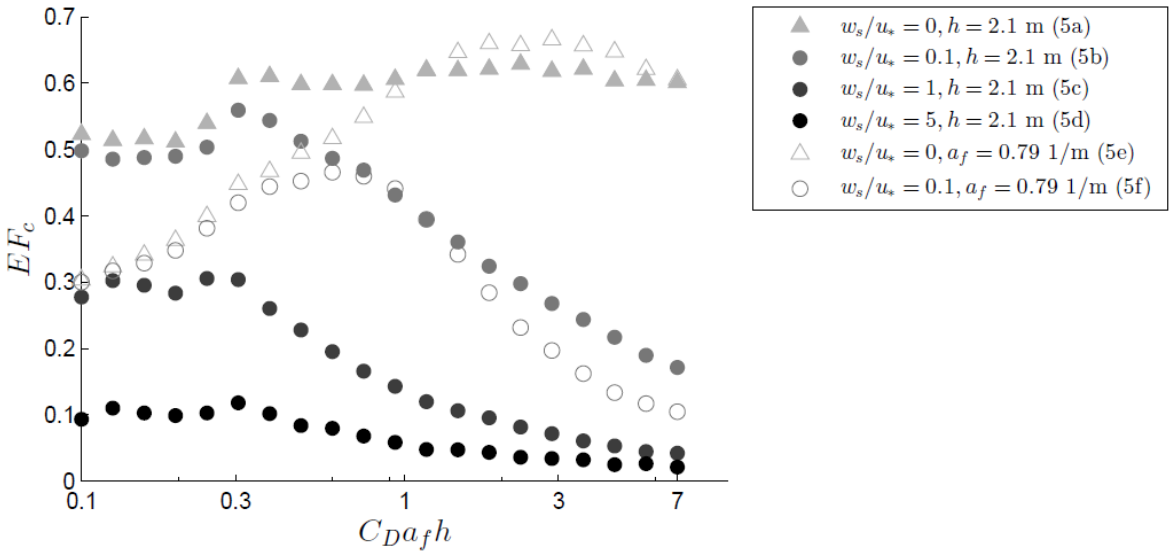

Figure 6 Canopy average escape fraction (EF_c) for canopies shown in Figure 5, as a function of the non-dimensional canopy density $C_D a_f h = 0.1 - 7$. Filled symbols denote canopies with $h = 2.1$ m and varying a_f; open symbols denote canopies with $a_f = 0.79$ m^{-1} and varying *h*.

Next, RDM was used to examine escape fraction over a range of canopy densities (Figure 5). Four values of velocity ratio were considered ($w_s/u_* = 0, 0.1, 1, 5$). To explore the individual influences of a_f and *h*, Figures 5a through 5d hold canopy height constant ($h = 2.1$ m) and vary $a_f = 0.07 - 4.9$ m^{-1}, but Figures 5e and 5f hold the frontal area constant ($a_f = 0.79$ m^{-1}) and vary $h = 0.19 - 13$ m. As expected, the escape fraction decreased with decreasing source height (z_{src}/h) in all cases. In addition, the escape fraction (EF) decreased as the settling velocity ratio (w_s/u_*) increased, illustrated by the progression from $w_s/u_* = 0$ to 5 (Figure 5a to 5d).

The trends with canopy density ($a_f h$) were clearly influenced by the penetration length scale, δ_e. The lower limit of the exchange zone ($z = h - \delta_e$) is indicated in each subplot by a thick black curve. Particles were more likely to escape if they originated above $z = h - \delta_e$. This trend was most clear for $w_s/u_* = 0.1$ and 1 (Figures 5b, c, f), for

497 which the contours of escape fraction track the line denoting δ_e. A similar relationship
498 would be expected for z_m, which is also a function of $C_D a_f h$, $z_m = \frac{1}{2}\delta_e$. For $w_s/u_* = 5$
499 (Figure 5d), the pattern was less obvious, because escape fraction was so low over
500 most of the canopy. In this case ($w_s/u_* = 5$), escape fraction was 0% over most of the
501 canopy, but rose to as much as 40% for particles originating above $h - \delta_e$. Generally,
502 for all particles with non-negligible settling velocity ($w_s/u_* = 0.1, 1, 5$), as the depth of
503 the region with elevated turbulence (δ_e) decreased ($C_D a_f h > 0.23$), the canopy average
504 escape fraction also decreased (circles in Figure 6). For these particles, both settling to
505 the ground and capture to the canopy were important mechanisms for detention within
506 the canopy, with the region $z_{src}/h \geq 0.5$ dominated by deposition on the canopy, and
507 the region $z_{src}/h \leq 0.5$ dominated by settling to the ground (data not shown).

508 Neutrally buoyant particles ($w_s/u_* = 0$) exhibited different escape behavior
509 (Figures 5a, f), because these particles could only deposit to the ground or to the
510 canopy via turbulent diffusion. For neutrally buoyant particles, the canopy average
511 escape fraction increased with increasing canopy density (triangles in Figure 6). This
512 can be explained by the trends in deposition by turbulent diffusion. At low values of
513 $C_D a_f h$, diffusivity was elevated across the full canopy height (Figure 2), so that particles
514 from any source height could reach the ground and deposit by diffusion. As $C_D a_f h$
515 increased, diffusivity within the canopy decreased (Figure 2), with a coincident decrease
516 in deposition to the ground, leaving more particles available to escape, so that canopy
517 average escape increased.

The trends in escape fraction were similar for constant *h* and constant a_f. For example, the difference in escape fraction (ΔEF) between each ($C_D a_f h$, z_{src}/h) pair in Figures 5a (constant h) and 5e (constant a_f) was $\Delta EF = 0.06 \pm 0.006(\mathrm{SE})$; between Figures 5b (constant h) and 5f (constant a_f), the difference in escape fraction was $\Delta EF = 0.08 \pm 0.006$ (SE). This demonstrated that escape was more strongly dependent on the non-dimensional parameter ($C_D a_f h$) than on the individual parameters of a_f and *h*. However, secondary influences from the individual contributions of a_f and h were apparent at low canopy density. Specifically, for $C_D a_f h \leq 0.5$ higher escape fractions were observed for the canopies with constant $h = 2.1$ m (Figure 6, solid symbols) than for the canopies with constant $a_f = 0.79$ m^{-1}, for which $h = 0.19 - 0.93$ m over the range $C_D a_f h = 0.1 - 0.5$ (Figures 6, open symbols). In other words, for the same value of $C_D a_f h$ higher escape fraction was observed for the taller canopy. This may be explained by the difference in the pseudo-velocity term ($\frac{dK_z}{dz}$) in eq. (2), which was larger for the taller canopies (data not shown). We caution, however, that this effect may arise from the oversimplified representation of the vertical profile of diffusivity. More detailed measurements of diffusivity profiles are needed to consider the real impact of the pseudo-velocity.

4. Conclusion

Forecasting infections from fungal disease can facilitate a reduction of fungicide application while maintaining crop yield (Aylor, 1999). This paper presented a practical

tool for predicting spore escape fraction, a required input to forecast the long-range transport of spores. The proposed RDM predicted escape fraction from a simple set of parameters [canopy height, canopy density, spore settling velocity, vegetation length scale, and wind speed] and did not require detailed velocity or turbulence measurements as input. The model was validated against field measurements of spore concentration downwind from a source within a maize canopy, and it was shown to perform as well as, or better than, more complex LES and LSM models. Although the RDM did not explicitly represent individual turbulent events (sweeps and ejections), it can predict escape fraction, because maximum particle escape, which was used to define escape fraction, occurred in the far-field, that is after transport over several integral time scales. The RDM demonstrated that escape fraction increased as canopy density ($a_f h$) decreased, as the settling velocity ratio (w_s/u_*) decreased, and as the source height (z_{src}/h) increased, confirming earlier studies (Aylor, 1990, Aylor, 1989, Aylor, 1999, Gleicher et al., 2014). The influence of the canopy density was largely reflected in the penetration length scale (δ_e), which segregated the canopy into regions of high and low escape probability. As a canopy matures, both canopy height and LAI increase, decreasing δ_e/h and creating a larger region within the lower canopy from which spore escape is inhibited.

Acknowledgements:

This material is based upon work supported by the National Science Foundation under Grant No. AGS-1005480. Any opinions, findings, or recommendations expressed in this material are those of the authors and do not necessarily reflect the views of the National Science Foundation

Works Cited

Andrade, D., Zaitao, P., Dannevik, W., and Zidek, J., 2009. Modeling soybean rust spore escape from infected canopies: Model description and preliminary results. J Appl Meteor Climatol 48, 789-803.

Aylor, D.E., 1982. Modeling spore dispersal in a barley crop. Agric Meteorol 26, 215-219.

Aylor, D.E., 1986. A framework for examining the inter-regional aerial transport of fungal spores. Agric For Meteorol 38, 263-288. Boundary-Layer Metorol 46, 257-273.

Aylor, D.E., 1989. Dispersion of spores released from an elevated line source within a wheat canopy.

Aylor, D.E., 1990. The role of intermittent wind in the dispersal of fungal pathogens. Annu Rev Phytopathol 28, 73-92.

Aylor, D.E., 2005. Quantifying maize pollen movement in a maize canopy. Agric For Meteorol 131, 247-256.

Aylor, D.E., 1999. Biophysical scaling and the passive dispersal of fungus spores: relationship to integrated pest management strategies. Agric For Meteorol 97, 275-292.

Aylor, D.E., Flesch, T.K., 2001. Estimating spore release rates using a Lagrangian stochastic simulation model. J Appl Meteorol 40, 1196-1208.

Aylor, D.E., Irwin, M.E., 1999. Aerial dispersal of pests and pathogens: implications for integrated pest management. Agric For Meteorol 97, 233-234.

Aylor, D.E., Taylor, G.S., 1983. Escape of *Peronospora tabacina* spores from a field of diseased tobacco plants. Phytopathol 73, 525-529.

Boughton, B.A., Delaurentis, J.M., 1987. A stochastic model of particle dispersion in the atmosphMere. Boundary-Layer Meteorol 40 (1), 147-163.

Chang, J.C., Hanna, S.R., 2004. Air quality model performance evaluation. Meterol Atmos Phys 87, 167-196.

Chamecki, M., 2013. Persistence of velocity fluctuations in non-Gaussian turbulence within and above plant canopies. Phys Fluids 25, 115110.

596 Denmead, O.T., Bradley, E.F., 1987. On scalar transport in plant canopies. Irrigation Sci
597 8, 131-149.

598 Durbin, P.A., 1983. Stochastic differential equations and turbulent dispersion. NASA
599 Reference Publication 1103.

600 Elskus, A.A., 2012. Toxicity, sublethal effects, and potential modes of action of select
601 fungicides on freshwater fish and invertebrates. U.S. Geological Survey Open-File
602 Report 2012-2013, at http://pubs.usgs.gov/of/2012/1213/.

603 Finnigan, J.J., 2000. Turbulence in plant canopies. Annu Rev Fluid Mech 32, 519-571.

604 Ghisalberti, M., 2009. Obstructed shear flows: similarities across systems and scales. J
605 Fluid Mech 641, 51-61.

606 Ghisalberti, M., Nepf, H., 2005. Mass transport in vegetated shear flows. Env Fluid
607 Mech 5, 527-551.

608 Ghisalberti, M., Nepf, H., 2006. The structure of the shear layer in flows over rigid and
609 flexible canopies. Env Fluid Mech 6, 277-301.

610 Gleicher, S., Chamecki, M., Isard, S.A., Pan, Y., Katul, G.G., 2014. Interpreting three-
611 dimensional spore concentration measurements and escape fraction in a crop canopy
612 using a coupled Eulerian-Lagrangian stochastic model. Agricultural and Forest
613 Meteorology 194, 118-131.

614 Grimmond, C.S.B., and Oke, T.R., 1999. Aerodynamic properties of urban areas
615 derived from analysis of surface form. J Appl Meterorol 38 (9), 1262-1292.

616 Hanna, S.R., 2003. Uncertainties in air quality model predictions. Boundary Layer
617 Meteorol 62: 3-20.

618 Harman, I.N., Finnigan, J.J., 2007. A simple unified theory for flow in the canopy and
619 roughness sublayer. Boundary-Layer Meteorol 123 (2), 339-363.

620 Hassid, S., 1983. Turbulent Schmidt number for diffusion models in the neutral
621 boundary layer. Atmos. Environ. 17(3), 523–527.
622
623 Isard, S.A., Russo, J.M., Ariatti, A., 2007. The integrated aerobiology modeling system
624 applied to the spread of soybean rust into the Ohio River valley during September 2006.
625 Aerobiologia 23, 271-282.

626 Israelsson, P.H., Y.D. Kim, E.E. Adams, 2006. A comparison of three Lagrangian
627 approaches for extending near field mixing calculations. Environ Model Softw 21, 1631-
628 1649.

629 de Jong, M.D., 1992. Risk assessment for the application of biological control of a forest
630 weed by a common plant pathogenic fungus. Risk Analysis 12, 465-466.

de Jong, M.D., Wagenmakers, P.S., Goudriaan, J., 1991. Modelling the escape of *Chondrostereum purpureum* spores from a larch forest with biological control of *Prunus-serotina.* Netherlands Journal of Plant Pathology 97, 55-61.

Koeltzsch, K., 2000. The height dependence of the turbulent Schmidt number within the boundary layer. Atmos. Environ. 34, 1147–1151.

Launder, B., 1976. Topics in Applied Physics, Vol. 12, Chapt. 6. Heat and Mass Transport. Springer-Verlag, 231–287.

Legg, B.J., and Powell, F.A., 1979. Spore dispersal in a barley crop: a mathematical model. Agric. Meterorol., 20: 47-67.

Luhar, M., Rominger, J., H. Nepf, 2008. Interaction between flow, transport, and vegetation spatial structure. Environ Fluid Mech 8, 423-439.

Massman, W.J., Weil, J.C., 1999. An analytical one-dimensional second-order closure model of turbulence statistics and the Lagrangian time scale within and above plant canopies of arbitrary structure. Boundary-Layer Meteorol 92, 81-107.

Nathan, R., Katul, G.G., 2005. Foliage shedding in deciduous forests lifts up long-distance seed dispersal by wind. Proc. Natl. Acad. Sci. U.S.A. 102 (23), 8251-8256.

Nepf, H.M., 2012. Flow and transport in regions with aquatic vegetation. Annu Rev Fluid Mech 2012 44, 123-142.

Nepf, H.M., M. Ghisalberti, B. White, E. Murphy, 2007. Retention time and dispersion associated with submerged aquatic canopies. Water Res Res 43, W04422.

Pan, Y., Chamecki, M., Isard, S.A., 2014. Large-eddy simulation of particle dispersion inside the canopy roughness sublayer. J Fluid Mech 753, 499-534.

Poggi, D., A. Porporato, L. Ridolfi, J. D. Albertson, G.G. Katul, 2004. The effect of vegetation density on canopy sub-layer turbulence. Boundary-Layer Meteorol 111, 565-587.

Raupach, M., 1994. Simplified expressions for vegetation roughness length and zero-plane displacement as functions of canopy height and area index. Boundary-Layer Meteorol 71, 211-216.

Raupach, M.R., Finnigan, J.J., Brunet, Y., 1996. Coherent eddies and turbulence in vegetation canopies: the mixing-layer analogy. Boundary-Layer Meteorol 78, 351-382.

Roberts, J.R., Reigart, J.R., 2013. Recognition and management of pesticide poisonings. 6th ed. United States Environmental Protection Agency, Office of Pesticide Programs, 272 pp. Available http://www2epa.gov/pesticide-worker-safety/recognition-and-management-pesticide-poisonings

667 Silva, P.S.L., Silva, K.M.B., Silva, P.I.B., Oliveira, V.R., Ferreira, J.L.B., 2012. Green ear
668 yield and grain yield of maize cultivars in competition with weeds. Planta Daninha 28
669 (1), 77-85.

670 Schlichting H., 1936. Experimental investigation of the problem of surface roughness.
671 NACA Technical Memorandum No 823.
672
673 Shaw, R.H., Tavangar, J., Ward, D.P., 1983. Structure of the Reynolds stress in a
674 canopy layer. J Clim Appl Meteorol 22, 1922-1931.

675 Tanino, Y. and Nepf, H.M., 2008. Lateral dispersion in random cylinder arrays at high
676 Reynolds number. J Fluid Mech 600, 339-371.

677 Thom, A., 1971. Momentum absorption by vegetation. QJR Meteorol Soc 97, 414-428.

678 Thomas, C., Foken, T., 2007. Flux contribution of coherent structures and its
679 implications for the exchange of energy and matter in a tall spruce canopy. Boundary-
680 Layer Meteorol 123, 317-337.

681 Wilson, J.D., Sawford, B.L., 1996. Review of Lagrangian stochastic models for
682 trajectories in the turbulent atmosphere. Boundary-Layer Meteorol 78, 191-210.

683 Wilson, J.D., Ward, D.P., Thurtell, G.W., Kidd, G.E., 1982. Statistics of atmospheric
684 turbulence within and above a corn canopy. Boundary-Layer Meteorol 24, 495-519.

685 Wilson, J.D., Yee, E., 2007. A critical examination of the random displacement model of
686 turbulent dispersion. Boundary-Layer Meterorol 125, 399-416.

687 Wilson, J.D., 2013. Turbulent Schmidt numbers above a wheat crop. Boundary-Layer
688 Meteorol 148, 255-268.